
NIAC PHASE I FINAL REPORT

DEEP MAPPING OF SMALL SOLAR
SYSTEM BODIES WITH GALACTIC
COSMIC RAY SECONDARY PARTICLE
SHOWERS

T. H. PRETTYMAN,¹ S. L. KOONTZ,² L. S. PINSKY,³ A. EMPL,³
D. W. MITTFELDLT,² B. D. REDDELL,² M. V. SYKES¹

¹PLANETARY SCIENCE INSTITUTE

²NASA JOHNSON SPACE CENTER

³UNIVERSITY OF HOUSTON

30-MAY-2014

2013 NASA INNOVATIVE ADVANCED CONCEPTS PHASE I PROJECT

GRANT NUMBER NNX13AQ94G

CONTENTS

Abstract	2
Introduction.....	3
Information from Galactic Cosmic Ray Showers	6
Asteroid Muography Concept.....	7
Production of Muons in Earth's Atmosphere.....	8
Scaling of Muon Production to Solid Surfaces	10
Sensitivity of Transmitted Muons to the Interior	13
Hodoscope Design Concepts	15
Pilot Radar-Muography Mission.....	18
Conclusions and Future Work.....	19
Acknowledgements	21
References	21

ABSTRACT

Galactic cosmic rays rain steadily from all directions onto asteroids and comets. The interaction of these high-energy ions produces a cascade of secondary particles, including muons, which can penetrate the solid interiors of small solar system bodies. Muons, which are produced in abundance in Earth's atmosphere, have been used to image large structures on Earth, including the Great Pyramids and the interior of volcanoes. In this study, we demonstrate that the transmitted flux of muons is sensitive to the interior density structure of asteroids and comets, less than a few hundred meters in diameter. Muonography has the potential to fill a critical gap in our knowledge of the deep interiors of small bodies, providing information needed for planetary defense, in situ resource utilization, and planetary science. We use Monte Carlo codes (MCNPX and FLUKA), which accurately model galactic cosmic ray showers, to explore systematic variations in the production of muons in solid surfaces. Results of these calculations confirm the scaling of muon production in Earth's atmosphere to solid regolith materials, as predicted by a simple, semi-empirical model. Muons are primarily produced in the top meter of the regoliths of asteroids and comets. Their rate of production is over three orders of magnitude lower than in Earth's atmosphere and depends strongly on regolith density. In practice, the use of muonography to characterize the interiors of small solar system bodies must overcome their low rate of production and their dependence on regolith density, which can vary over the surface of asteroids and comets. We show that interior contrast can be resolved using a muon telescope (hodoscope) with about 1 m² aperture with integration times ranging from hours to weeks. Design concepts for a practical hodoscope that could be deployed in situ or on an orbiting spacecraft, are described. Regolith density within the top meter of an asteroid can be determined from radar observations. A concept for a pilot mission that combines remote radar measurements with in situ muonography of a near-Earth asteroid is presented. Perceived challenges and next steps for the development of the concept are described.

INTRODUCTION

What if we could look inside an asteroid or comet? Information about the internal density structure of these small solar system bodies would provide powerful constraints on their formation and evolution as well as information needed for planetary defense, mining, and in situ resource utilization (ISRU). For example, physical processes within cometary nuclei are poorly understood (Weissman et al., 2004). Characterization of their interior could provide new insights into volatilization and venting mechanisms. Small asteroids (< 1 km diameter) may be unconsolidated blobs of rubble or monolithic blocks ejected from a larger, parent body (e.g. Fujiwara et al., 2006). Determining the bulk physical properties and interior structure of meteoroids is both important for understanding their origins and crucial in formulating strategies for planetary defense (e.g., Ahrens and Harris, 1992; Asphaug et al., 1998). The Torino scale, which provides a measure of impact hazard from near Earth objects (NEOs), sets a lower limit of concern for meteoroids about 20 m in diameter (Binzel, 2000). This is about the size of the Chelyabinsk meteoroid (Brown et al., 2013), which punctuated the hazard posed by relatively small objects. At present, asteroid Toutatis (1.9- × 2.4- × 4.6-km) is the largest known potentially hazardous object (PHO) (Hudson and Ostro, 1995; NASA NEO Program). Finally, asteroids contain a “gold mine” of diverse materials that could be exploited by our space-faring civilization (e.g. Hartman, 1985; Kargel, 1994; O’Neill, 1977; Longman, 2013). The ability to image the interior of asteroids would facilitate profitable and efficient exploitation of this potential resource.

At present, the internal structure of small bodies must be inferred from surface morphology (e.g. as observed by photographic imagery or radar) and indirectly from other observations. For example, radar measurements can provide information about the density structure of the regolith to depths of about a meter (e.g. Magri et al., 2001). The rubble-pile structure of Itokawa was inferred from its appearance (presence of boulders and blocks) and bulk density (Fujiwara et al., 2006). The pattern of debris produced by tidal disruption of the comet Shoemaker-Levy 9 by Jupiter is consistent with a rubble-pile (Weissman et al., 2004) (Fig. 1). Imagery of the nucleus of 81P/Wild 2 by NASA/Stardust is also suggestive of a rubble-pile structure (ibid.).

Our prospective method to directly map the interior of asteroids and comets was first

developed to image large structures, both natural and synthetic, on Earth’s surface. Dubbed cosmic ray “muography” by H. K. M. Tanaka and colleagues, this method makes use of atmospheric muons – relativistic leptons produced by galactic cosmic ray showers in Earth’s atmosphere (e.g. Gaisser, 1990) – to radiograph large objects. These long-range, penetrating particles were used by Alvarez et al. (1970) to search for hidden chambers in the Great Pyramid of Giza. More recently, muons

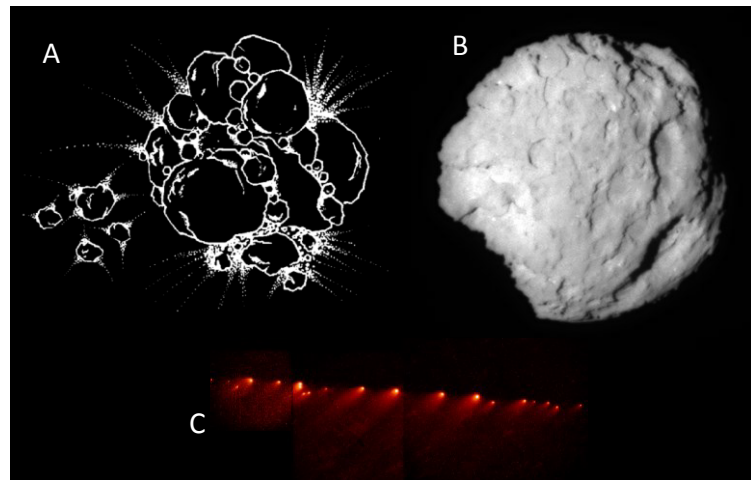


Figure 1. A) Artist’s conception of a rubble-pile cometary nucleus (from Weissman et al., 2004); B) Blocky surface of 81P/Wild 2 (NASA/Stardust); C) Breakup of Shoemaker-Levy 9 (NASA/HST) .

have found application in imaging cargo containers for homeland security (Borozdin et al., 2003), the damaged cores of the Fukushima Daiichi reactors (Borozdin et al., 2012; Miyadera et al., 2013), and in archeology (Menichelli et al., 2007). Muography has also been applied to map the interior of geologic structures, such as volcanoes using radiographic and tomographic methods (Fig. 2) (Tanaka et al. 2007, 2008, 2009, 2010a, 2010b; Lesparre et al., 2010; Marteau et al., 2012; Tanaka, 2012; Okubo and Tanaka, 2012; Ambrosino et al., 2014). The inspiration for this project is primarily the work of Tanaka and colleagues on transmission imaging of geologic structures (ibid.).

Muography is effective at Earth's surface because the flux of atmospheric muons is high and their energy-angle distribution is thoroughly understood (e.g. Allkofer et al., 1971). The flux of muons at sea level is second only to neutrinos. The vertical muon intensity is about $100/\text{m}^2/\text{sr}/\text{s}$ for muons with momenta greater than $200 \text{ MeV}/c$ (ibid.). Here and elsewhere in this report, the vertical muon intensity refers to the inward directed muon flux (antiparallel to zenith). Like electrons, muons are singly-charged particles that undergo weak interactions, transferring energy via radiative processes and multiple Coulomb scattering; however, since they are more massive than an electron they travel further through matter. At relativistic energies, their decay length exceeds their range. Atmospheric muons have been detected in mines, several kilometers deep (e.g. Bugaev et al., 1998). Ionization by the passage of muons is readily detected by very simple sensors (e.g. coincidence events between two scintillating paddles). As a result, muon detectors are easy to make and fundamental experiments can be carried out at low cost in high school and undergraduate classrooms (e.g. Coan et al., 2006; Goldader and Choi, 2010).

The application of muography to the geophysical characterization of solar system bodies other than Earth is still in the concept phase. For example, Kedar et al. (2013) proposed a compact muon hodoscope to image surface features on Mars. The horizontal flux of atmospheric muons at the martian surface was estimated to be larger than that of Earth, providing ample intensity for radiography (ibid.). The atmosphere of Mars is relatively thin such that the primary GCRs and secondary particles other than muons will also trigger the detector; however, only the muons will

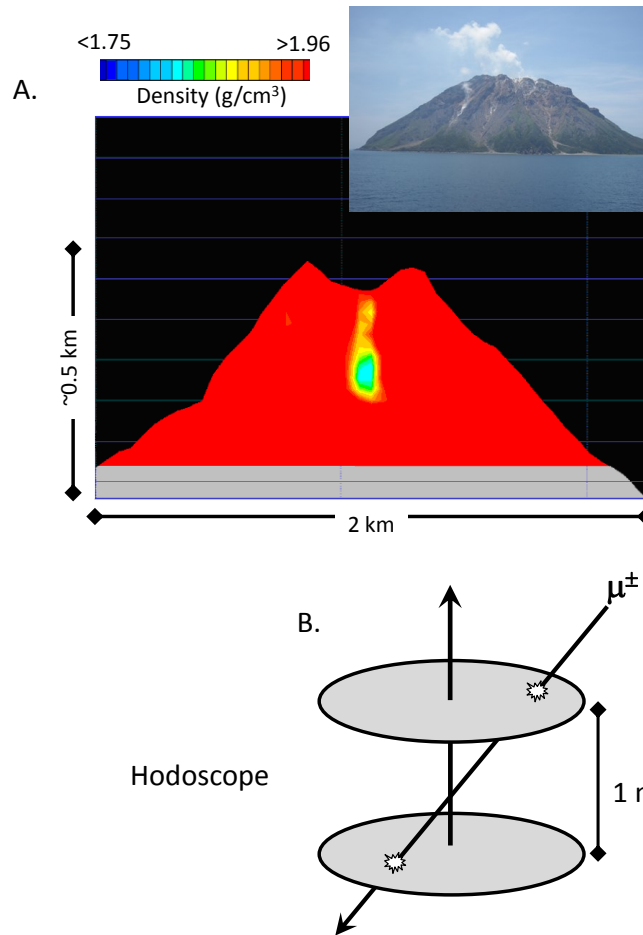


Figure 2. A) Internal structure of the Satsuma-Iojima volcano using a 1 m^2 muon telescope (hodoscope) by Tanaka et al., 2010a, 2010b. B) Conceptual diagram of a hodoscope consisting of two, position-sensitive, scintillating layers. A muon (μ^\pm) that transects the hodoscope will produce two flashes of sensible light in coincidence. The incident direction of the muon is determined from the positions of the interactions.

traverse an intervening geological feature (volcano, mountain, etc...). If the attenuated muon flux overwhelms the flux of secondary charged particles produced near the surface within the field of view of the hodoscope, then relative variations in the measured image inside the shadow of the feature can be attributed to muons penetrating the target. The variations will convey information about the internal structure of the intervening object. A slight upward orientation of the muon detector would prevent particles, other than those scattered in the surface, from entering the hodoscope from the opposite direction of the target. Based on this cursory assessment, it seems reasonable that a simple hodoscope design that works for Earth applications could be deployed on Mars with some modest modifications.

The extension of muography to small, airless bodies is complicated by the fact that muons are made in the solid surface, which is irregular and, unlike Earth's atmosphere, may vary widely in composition and density as a function of position on the surface (e.g. Fujiwara et al., 2006; Veverka et al., 2001). Moreover, muons are produced by the decay of mesons (primarily charged pions and kaons, π^\pm and K^\pm). Within a solid surface, it is more likely that these mesons will collide before they have a chance to decay. Consequently, the production of muons in solid surfaces will be strongly suppressed relative to Earth's atmosphere. Finally, the hodoscope will be exposed to primary GCRs as well as secondaries produced near the surface on the same side of the object as the hodoscope. In contrast to the Mars application, it is not obvious that this scattered, secondary charged particle flux will be small in comparison to the flux of muons that penetrate the asteroid. In addition, contributions from primaries that penetrate the hodoscope from the direction opposite the asteroid must be rejected. These factors must be considered when designing a hodoscope for small, airless bodies.

The objective of this study is to assess the feasibility of using muons and other secondary products of GCR showers to image the interior structure of small, airless bodies. The project team has expertise in cosmic ray physics, meteoritics, and planetary remote sensing. Members of the team use general purpose radiation transport codes, MCNPX (e.g. McKinney et al., 2006; Pelowitz et al., 2011) and FLUKA (e.g. Ferrari et al., 2005; Battistoni et al., 2007, 2008; Kalmykov et al., 2011), for accelerator, space dosimetry and planetary science. These codes enable very detailed modeling of galactic cosmic ray showers. MCNPX and FLUKA can determine the production of secondary particles in solid surfaces in space to assess the magnitude of prospective signatures and interfering backgrounds. Results of detailed modeling are used to scale a semi-empirical model of muon production from Earth's atmosphere to the solid surfaces of airless bodies. The semi-empirical model is used to determine the sensitivity of muons to the interior structure of asteroids and comets. The possibility of using high energy muons produced by the decay of charmed mesons to

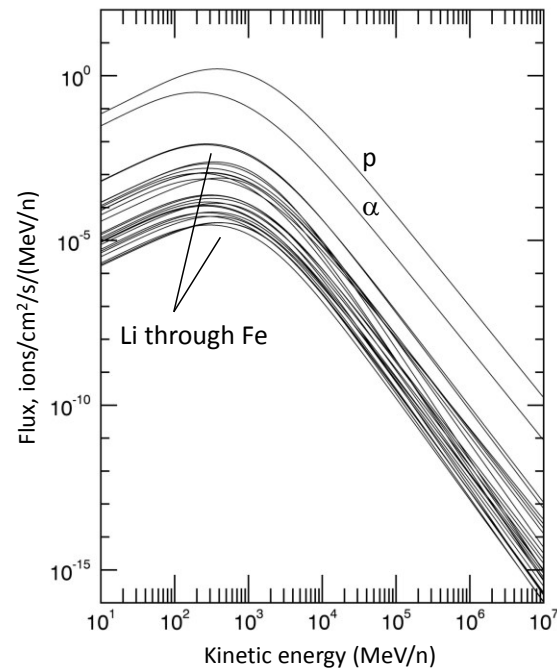
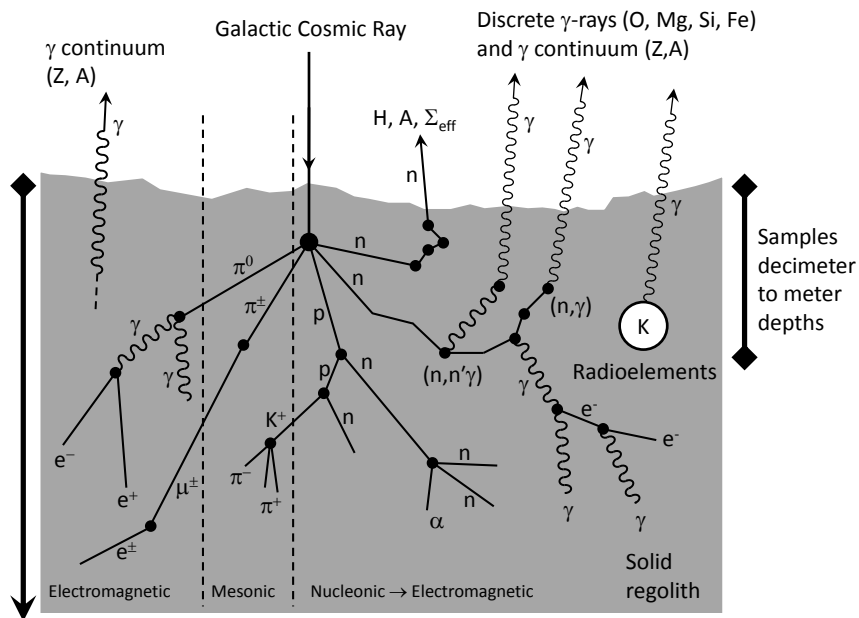


Figure 3. Differential flux of GCR protons (p), alpha particles (α), and ions $Z=3, \dots, 26$. About 86% of GCR nucleons are in the form of protons and alpha particles.



μ^\pm (muons) can penetrate to km depths

Figure 4. Schematic diagram of a galactic cosmic ray interaction with the solid surface (regolith) of an airless body. Signatures presently used for chemical remote sensing of planetary surfaces are indicated. Neutrons provide information about the hydrogen content, neutron absorption cross section, and atomic mass of the regolith. Discrete gamma rays produced by nuclear reactions provide a fingerprint that can be analyzed to determine the abundance of rock forming elements. Continuum gamma rays also convey information about the atomic number and atomic mass of the regolith. Gammas produced by the decay of natural radioelements (e.g. K) are also measured.

map the interior of small bodies is discussed. A qualitative discussion of hodoscope design is presented along with a pilot mission concept. Perceived limitations of the method and next steps are described.

INFORMATION FROM GALACTIC COSMIC RAY SHOWERS

Galactic cosmic rays (GCRs) are ions that have been accelerated to very high energy by processes occurring outside of our solar system. The exact details of their production and acceleration mechanisms are the subject of ongoing research; however, their composition and energy distribution at 1 AU is well known (Fig. 3; Badhwar and O'Neill, 1996). At kinetic energies lower than a few GeV, the flux of GCRs that penetrate the heliosphere is modulated by strength of the solar magnetic field, which has a 12 year cycle. At higher energies, the distribution of GCRs is unaltered by interactions with the heliosphere.

Solar system bodies are exposed to a steady rain of GCRs, which arrive uniformly from all directions. When they enter Earth's atmosphere they trigger a shower of secondary particles, including nucleons, mesons, leptons, and neutrinos, some which reach the surface of the Earth. The interaction of GCRs with a solid asteroid surface is illustrated in Fig. 4, which shows the components of the GCR shower (nucleonic, mesonic, and electromagnetic). GCRs produce a cascade of protons (p), neutrons (n), and ions, which undergo subsequent interactions, including

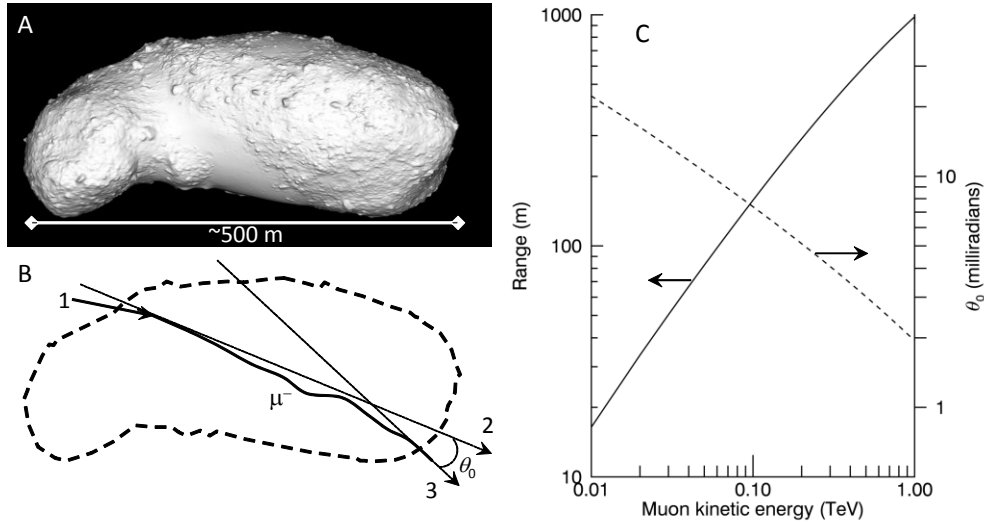


Figure 5. A) Orthographic projection of a shape model (Gaskell et al., 2008) of the rubble-pile asteroid 25143 Itokawa (Fujiwara et al., 2006), rendered using the methods described by Prettyman et al. (2011). B) Cartoon illustrating the path of a high-energy muon (μ^-) through the asteroid. Muon production is initiated by the interaction of a galactic cosmic ray near the surface of the asteroid (1). The muon traverses the asteroid undergoing many collisions before exiting the other side. The final direction (3) of the muon as it escapes into space deviates from its initial direction (1) due to scattering processes. The magnitude of the deviation (r.m.s. deflection, θ_0) depends primarily on the initial energy of the muon and the amount of rocky material traversed. C) Small deviations are expected for muons in the 10-GeV to TeV range, many of which can penetrate Itokawa.

nuclear reactions that make gamma rays (γ) and electrons (e^\pm). In addition, mesons, primarily pions (π^0, π^\pm) and kaons (K^\pm) are produced in high energy collisions. These decay to produce muons (μ^\pm), the long-range charged component of the cosmic ray shower. After undergoing collisions, some of the secondary particles arrive at the surface and escape into space. These are primarily gamma rays and neutrons; however, the other particles are included in the leakage flux. As described in Fig. 4, the escaping gamma rays and neutrons convey chemical information about the top few decimeters of the surface (e.g. Lingenfelter et al., 1961; Harrington et al., 1974; Feldman et al., 1998; Feldman et al., 2000; Evans et al., 2001; Boynton et al., 2002; Prettyman et al., 2004, 2011, 2012; Yamashita et al., 2012; Lawrence et al., 2013).

ASTEROID MUOGRAPHY CONCEPT

The stopping power for muons is determined by ionization (multiple Coulomb scattering) and radiative losses (pair production, bremsstrahlung, and photonuclear interactions). Their range depends on the atom density and the effective atomic number of the material they traverse. The mean distance to decay is proportional to the kinetic energy of the muons (about 6 km at 1 GeV) (Tanaka et al., 2008), which for relativistic muons is longer than their range in planetary materials. Thus, the flux of muons arriving at a detector depends on their initial kinetic energy distribution, the density and composition of the material traversed, and target thickness. The primary contrast

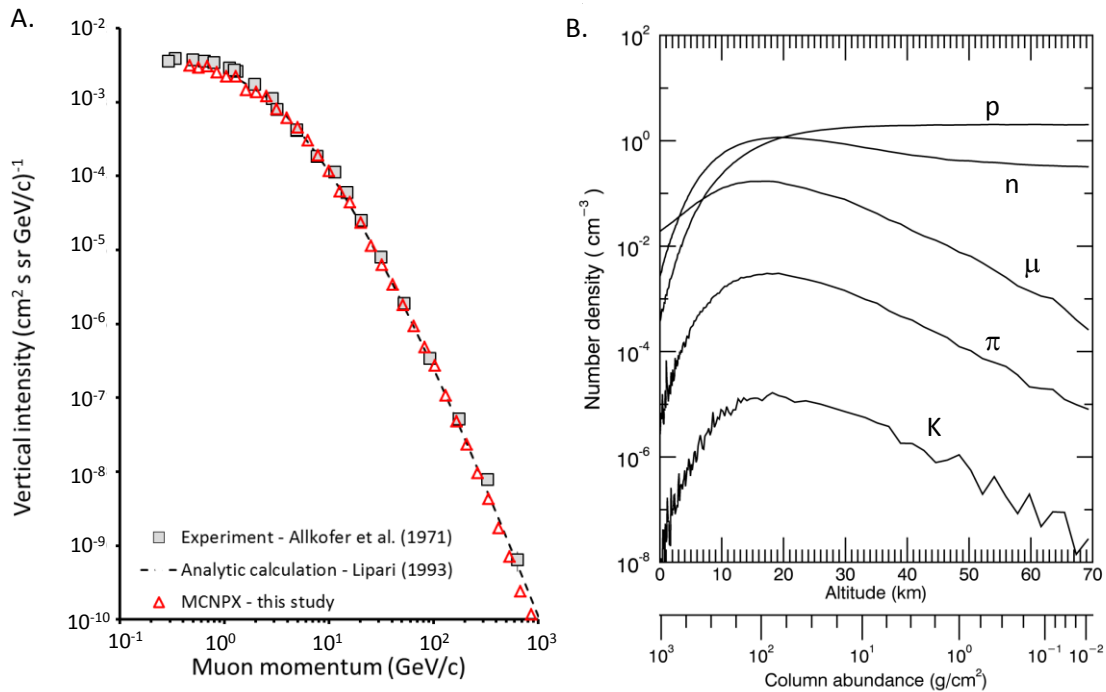


Figure 6. A) The vertical muon flux at sea level determined by analytic model and MCNPX is compared to experimental data; B). The number density of selected particles calculated by MCNPX is plotted as a function of altitude and column abundance.

mechanism for muon imaging is simply the removal of lower energy muons that do not penetrate the target.

As illustrated in Fig. 5, muons in the 10-GeV to 1-TeV range can penetrate small asteroids (10s of meters to about a kilometer in diameter). Estimates of their deflection due to multiple scattering indicate that better-than-meter-scale intrinsic spatial resolution could be achieved using muon radiography. Muons are preferentially produced in the direction of the cosmic ray primary. Thus, muons are produced in the regolith on the opposite side of the asteroid from which measurements are made. The flux of muons in any selected direction varies with the total column (kg/m²) of materials traversed. Since the asteroid shape is known, the chord-length (km) traversed can be determined, enabling an estimate of internal density. Measurements of the flux at many different locations and directions (e.g. from orbit) would enable tomographic reconstruction of the interior density distribution; however, knowledge of the shape of the object and a thorough understanding of the muon source characteristics is needed (Prettyman et al., 2014; Miller and Lawrence, 2014).

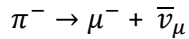
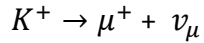
PRODUCTION OF MUONS IN EARTH'S ATMOSPHERE

Since muon production in Earth's atmosphere is known, we validated one of our modeling codes, MCNPX, against measurements of the vertical muon flux at sea level. The atmosphere was modeled as uniform in composition (78.084% N₂, 20.946% O₂, 0.934% Ar, and 0.0387% CO₂, by volume). Assuming a mean temperature of 240K, the scale height was determined to be 7 km. The atmosphere vertical density structure was modeled using concentric spheres, with constant column

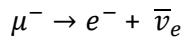
abundance and increasing in thickness with altitude as determined by the scale height. The reference altitude (top of the atmosphere) was taken to be 70 km. The total column was 1030 g/cm². The GCR flux was modeled as isotropic, incident on the reference surface. Protons and alpha particles were treated using the Badhwar-O'Neill 2011 model (Fig. 3), with kinetic energies ranging from 10 MeV/n to 10 TeV/n. For this study, MCNPX was modified to transport particles greater than 1 TeV/n. A combination of the Cascade Excitation Model (CEM) and the Los Alamos Quark-Gluon String Model (LAQGSM) was used to model high energy interactions (Mashnik et al., 2006). These models treat all stages of high energy reactions induced by galactic cosmic rays (the intranuclear cascade, pre-equilibrium, evaporation and fission, and de-excitation of residual nuclei).

A comparison between the MCNPX-calculated sea-level vertical intensity and experimental data (Allkofer et al., 1971) is shown in Fig. 6. An analytical calculation by Lipari (1993) is also shown. The MCNPX-calculated vertical intensity is broadly consistent with the data and analytic model. The number density of charged and neutral particles has a broad maximum at around 15-20 km altitude, consistent with the location of the Pfofzter maximum (Pfofzter, 1936) (Fig. 6B). Of the particles plotted, the muon flux is highest at sea level. Muons have very small interaction cross sections and are comparatively long lived. Thus, their population decreases more slowly at low altitude than the nucleons and mesons, which are lost to decay and collision in the troposphere. The dearth of pions and kaons at sea level indicates that most muon production is in the atmospheric column.

Mesons are produced in high energy collisions and decay to produce muons and their neutrinos:



Muons subsequently decay to produce electrons and electron neutrinos, e.g.



In Earth's atmosphere, most muons are made by pion and kaon decay; however, muons are also made by the decay of very short lived, charmed hadrons (primarily D mesons that contain the charm quark). These "prompt muons" have not been observed experimentally, but are thought to be more abundant at high energy (> 100 GeV) than muons produced by pion and kaon decay. As we shall see, muons from the decay of charmed mesons may be a major component of the muon flux in solid surfaces. Particle decay constants are compared in Table 1.

Table 1. Particle decay constants. Decay length is obtained by multiplying the decay constant by the Lorentz factor γ (tabulated values are from Gaisser, 1990).

Particle	Decay constant $c\tau_0$ (cm)
μ^\pm	6.6×10^4
π^\pm	780
K^\pm	371
D^\pm	0.028

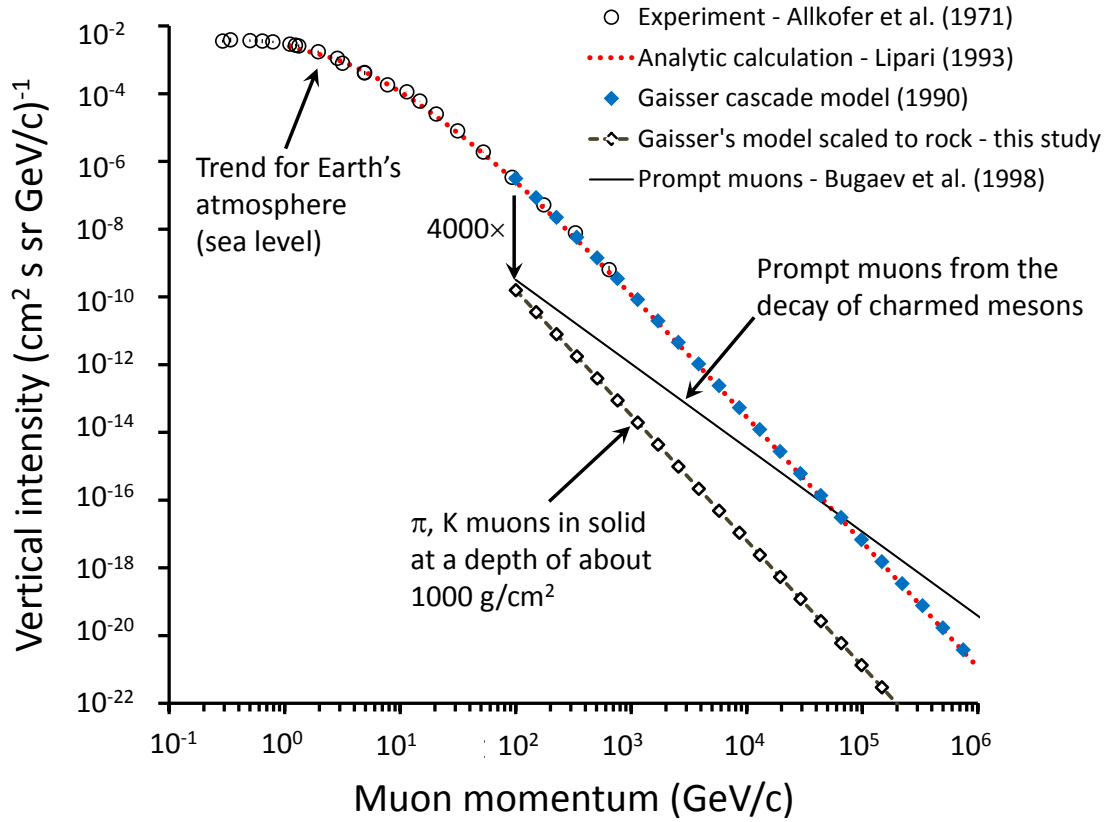


Figure 7. The Gaisser cascade model of the vertical muon flux at sea level on Earth is scaled to a solid with a density of 1.6 g/cm^3 , typical of planetary regolith materials. Muon production in the top layer of an asteroid by the decay of pions and kaons is over three orders of magnitude less than in Earth's atmosphere. A prompt component from the decay of charmed mesons does not depend on density.

SCALING OF MUON PRODUCTION TO SOLID SURFACES

An approximate scaling of muon production with density can be derived using a semi-empirical cascade model popularized by Gaisser (1990), in which muon production is modeled as a balance between meson collisional losses and decay. The contribution to the vertical differential flux of muons at sea level for each meson meson ($m = \pi, K, D, \dots$) has the following functional form:

$$\varphi_m(E) = aE^k \left[\frac{A_m}{1 + B_m E/\varepsilon_m} \right] \text{ muons}/(\text{cm}^2 \text{ s sr GeV}) \quad (1)$$

where E is muon energy (GeV). The term E^k is proportional to the flux of primary galactic cosmic ray nucleons. A_m is proportional to the spectrum-weighted moment of the nucleon-pion cross section; B_m is a function of the ratio of meson to nucleon attenuation lengths. To first order, both

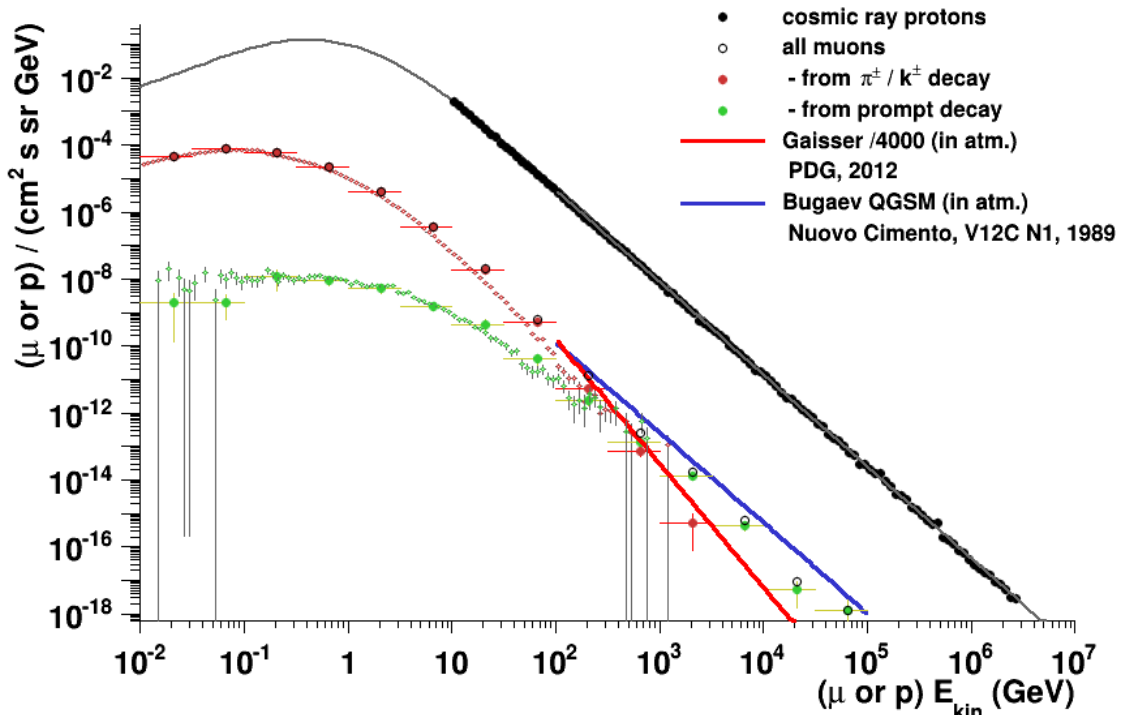


Figure 8. The vertical flux of muons at a depth of 1000 g/cm² in a solid asteroid regolith as calculated by FLUKA. The results of two calculations are shown: the first (small symbols) is for analog sampling of the energy distribution of the source (GCR protons, in black); the second (large symbols) is for biased sampling of the source, wherein high energy protons are preferentially sampled and weighted. The total muon flux is shown along with contributions from the decay of π , K mesons and the decay of charmed mesons (prompt component). The FLUKA simulations are compared to the Gaisser cascade model, scaled to rock, and Bugaev's model of prompt muons (cf. Fig. 7). Note that the abscissa is particle kinetic energy.

of these terms depend on the chemical composition of the medium. The term E/ε_m is the decay length of the meson (m), given by $d_m = \rho \gamma (c \tau_0)_m$, where ρ is density (g/cm³). The numerical values of the parameters of Eq. 1 are $a=0.14$, $k=-2.7$, $A_\pi = 1$, $B_\pi = B_K = 1.1$, $\varepsilon_\pi = 115$, $A_K = 0.054$, and $\varepsilon_K = 850$ (Gaisser, 1990). We assume that the decay constant for charmed mesons is small enough that they will decay before colliding. Thus, the density effect for these short lived particles will be ignored. In other words, prompt muon production in the surface of an asteroid is expected to be about the same as in Earth's atmosphere.

As shown in Fig. 7, the Gaisser model is a good match to an analytical calculation by Lipari (1993) above 100 GeV, which, in turn, matches the experimental trend at lower energies (Allkofer et al., 1971). Scaling the flux with density is accomplished by multiplying the E/ε_m term of Eq. 1 by the ratio of the density of the solid material to the mean density of Earth's atmosphere at a depth of 200 g/cm² where the muons are produced (about 3×10^{-4} g/cm³) (Gaisser, 1990). Fig. 7 shows the scaled, vertical muon flux for a solid density of 1.6 g/cm³, which is typical of a planetary regolith. The effective depth is equivalent to sea level on Earth (1000 g/cm²). The muon flux scaled to regolith densities is over three orders of magnitude smaller than the flux of muons at sea level on

Earth. In a planetary regolith, we expect that the flux of prompt muons will be higher than muons from π , K decay for energies greater than 100 GeV. At lower energies, the π , K muon component will be dominant.

To verify this picture, the FLUKA code was used to model the production of muons in a solid asteroid. FLUKA is based on verified microscopic models of physical processes which, like MCNPX, provide a thorough treatment hadron-hadron interactions, the production and decay of mesons and their progeny. For a description of the hadron interactions implemented in FLUKA see Fass et al. (1995, 2000), Ferrari and Sala (1998) and Battistoni et al. (2006). The list of particles modeled by FLUKA includes charmed mesons, which decay to make prompt muons. The asteroid composition was modeled as “standard rock” (Note that 20 wt.% FeO, 80 wt.% SiO₂ approximates standard rock, which is defined as a material with Z=11, A=22, A/Z=2 and Z²/A=5.5. The values for our material are respectively, 11, 22.3, 2.01, and 5.43.). The density of the asteroid was 1.6 g/cm³, a value typical of planetary soils.

Fig. 8 shows the vertical flux of muons at a depth of 1000 g/cm² within the asteroid as modeled by FLUKA for GCR protons (from the Badhwar-O’Neill model, as shown in Fig. 3 and Fig. 8). The FLUKA calculation confirms the semi-empirical scaling of muons produced by π , K mesons (cf. Fig. 7). In addition, the calculation predicts a prompt component similar to that calculated by Bugaev et al. (1998) for Earth’s atmosphere. The prompt component exceeds the π , K component between 100 GeV and 1 TeV. Here, it is important to note that there is great uncertainty in the magnitude of muon production by charmed mesons. This component has not been detected for natural cosmic ray sources at Earth due to interfering contributions from π , K muons; however, we expect that prompt muon production will be characterized in future accelerator experiments.

Having confirmed the semi-empirical scaling of π , K muons with density, we are presented with yet another challenge. Unlike Earth’s atmosphere, the regolith of asteroids and comets is not homogeneous. On Eros, there are extensive smooth, ponded regions, likely having low regolith density, and other blocky regions that will have higher density (see Fig. 5; Veverka et al., 2001). A density variation between 1.6 g/cm³ and about 3 g/cm³ for blocks of silicate materials could be found on small asteroids. The approximately 1/ ρ variation in muon production implied by our semi-empirical scaling suggests a factor-of-two variation between these end-members. On a comet, where ice is mixed with silicate minerals, the variability in muon production may be larger. In a muon radiograph, the interior of the object may be obscured by density variations in the outer surface.

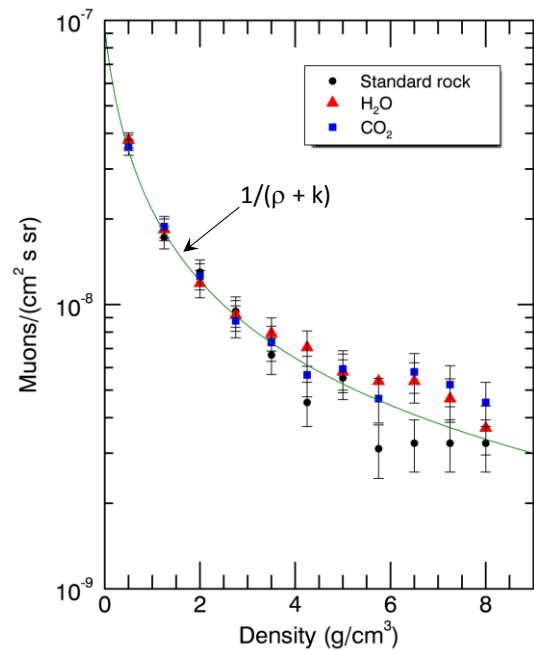


Figure 9. The integral vertical (downward-directed) muon intensity at a depth of 1000 g/cm² for muons with kinetic energies greater than 50 GeV. MCNPX calculated intensities are shown as symbols with 1 σ error bars, representing the statistical uncertainty of the Monte Carlo calculation. The trend with density (ρ) was fitted by eye (k is a fitted constant).

MCNPX simulations of the muon integral flux ($E_\mu > 50$ GeV) as a function of regolith density for three compositions are shown in Fig. 9. Although the range of densities is nonphysical, the simulations demonstrate that the intensity of muons varies inversely with density. In addition, any compositional effect appears to be small relative to variations within the range of densities expected for small-body regoliths. Since the production of secondary hadrons and mesons depends on the atomic number and mass of the target, compositional variations may be more prominent for asteroids with significant metal content.

SENSITIVITY OF TRANSMITTED MUONS TO THE INTERIOR

Using the results from our scaling study, we carried out simulations to estimate the sensitivity of transmitted muons to density variations within an asteroid or comet. As illustrated in Fig. 10, the asteroid and the inclusion were modeled as concentric spheres. The muon source (μ_{in}) was distributed uniformly on a sphere (S) at 1000 g/cm^2 depth. The angular distribution was assumed to be the same as that of the incident GCR protons. Namely, the inward angular distribution of muons was linear in the cosine of the emission angle relative to the sphere's normal direction at the emission site (equivalent to an isotropic source far from the asteroid). The transport of muons within the asteroid was modeled by MCNPX, which accounts for all mechanisms affecting muon transport (multiple Coulomb scattering, radiative losses, and pair production) and their decay. The current of muons escaping from the outer surface of the asteroid (μ_{out}) was tallied as a function of kinetic energy and the cosine of escape angle (θ) relative to the sphere normal direction at the location of escape.

Sensitivity calculations were carried out for an ideal hodoscope, capable of counting every

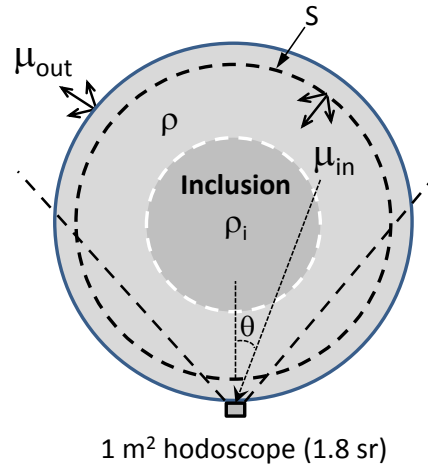


Figure 10. Geometry for simulations of the response of a hodoscope positioned on the surface of an asteroid to the presence of an interior inclusion. The density of the outer portion of the asteroid is ρ . The density of the inclusion is ρ_i . The muons were assumed to be produced 1000 g/cm^2 beneath the surface with the same angular distribution as the GCRs incident on the asteroid.

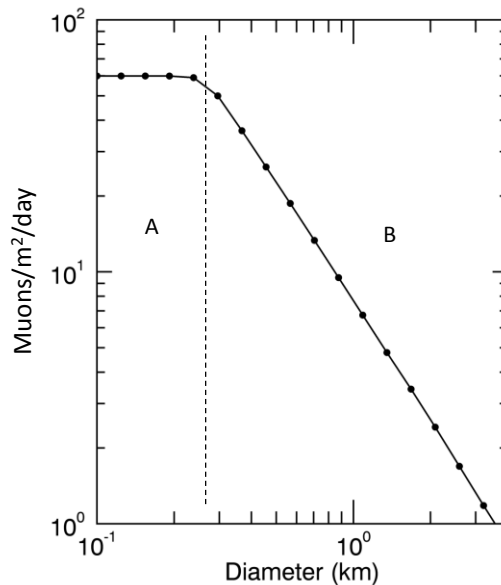


Figure 11. Integral leakage current of muons as a function of asteroid diameter for prompt muons with energies greater than 0.1 TeV (see Fig. 7). Muons in this energy range punch through asteroids with diameters less than about 200 m (A). For larger asteroids, a portion of muons are stopped within the asteroid, resulting in a gradual decrease in leakage current with diameter (B).

incident muon separately from all sources of background. For maximum signal, the hodoscope was assumed to be deployed on the surface of the asteroid. Results are reported for a hodoscope with a 1 m² aperture, similar to that used by Tanaka et al. (2010b) for Earth applications.

To illustrate the nature of charged-particle range radiography, we assumed that our source was prompt muons only, with energies greater than 0.1 TeV (Bugaev, 1998; Fig. 7). For uniform asteroids ($\rho = \rho_i = 2 \text{ g/cm}^3$), these muons will punch through asteroids with diameters less than about 200 m (region A of Fig. 11). For larger asteroids, a portion of the muons will be stopped within the asteroid. As the asteroid diameter increases, more of the muons are stopped. Thus, the leakage current of prompt muons steadily decreases with asteroid diameter (region B of Fig. 11).

To visualize the response of transmitted muons to internal density changes, consider an 800-m diameter asteroid with a 400-m inclusion. The ideal hodoscope is assumed to be capable of binning the detected muons with direction, as a function of the cosine of the angle of incidence (θ). The angular response of the hodoscope is shown in Fig. 12 for inclusion densities ranging from 0.5- to 3.6-g/cm³. The incident cosines for muons passing directly through the inclusion range from 0.87 to 1. The counting rate within this range varies with inclusion density. Outside this range (<0.87) the counting rate does not depend on density. The transmitted signal from prompt muons is sensitive to the density of a large inclusion; however, the counting rate for transmitted muons is quite low.

The amount of time required to detect a change in density in the interior region can be estimated by defining the signal to be the relative change in counts within the field of view occupied by the inclusion ($Counts_{FOV}$) to that which would be observed for a homogenous asteroid ($Counts_{Hom.}$) (see Fig. 12):

$$Signal = \frac{Counts_{FOV} - Counts_{Hom.}}{Counts_{Hom.}} \quad (2)$$

The 3σ Poisson detection limit for the inclusion can be expressed in terms of mean counting rates:

$$Time > \frac{9 \times Rate_{FOV}}{(Rate_{FOV} - Rate_{Hom.})} \quad (3)$$

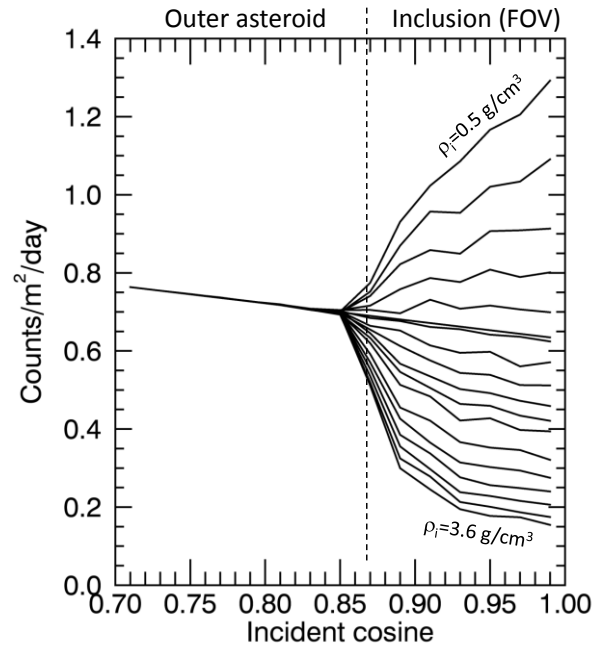


Figure 12. Counting rate as a function of the cosine of the angle of incidence of muons on a 1 m² hodoscope. The response for muons transmitted through an 800-m diameter asteroid with a 400-m diameter inclusion. The density of the inclusion was varied from 0.5 g/cm³ to 3.6 g/cm³ in 18 steps. The density of the material outside the inclusion (“outer asteroid”) was 2 g/cm³. The counts within the field of view containing the inclusion monotonically decrease with increasing inclusion density.

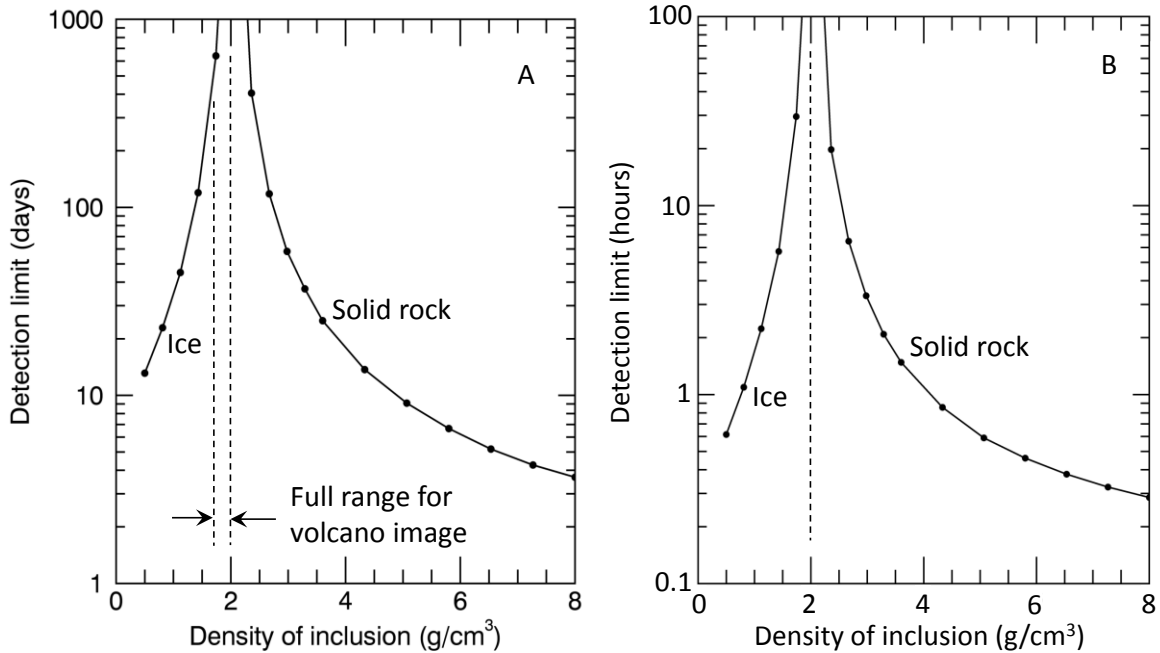


Figure 13. Detection limit for an inclusion within a small body (asteroid or comet) as a function of inclusion density. The density of the outer portion of the asteroid is 2 g/cm^3 . Case A is for prompt muons ($> 0.1 \text{ TeV}$) produced in an 800-m diameter asteroid with a 400-m diameter inclusion. Case B is for muons ($> 10 \text{ GeV}$) produced by the decay of pions and kaons in a 50-m diameter asteroid with a 20-m diameter inclusion. The full range of densities in the volcano image of Fig. 2 is shown for comparison (left).

The detection limit for prompt muons is plotted as a function of inclusion density in Fig. 13A. For small changes in density, similar to that observed by Tanaka et al. (2010a, 2010b) within Satsuma-Iojima volcano (Fig. 2), hundreds of days would be required to detect the inclusion. However, there is reason to believe that the contrast range for small bodies might be relatively high. For example, they may incorporate ice, metal-rich regions, or solid blocks of rock. The contrast between ice or rock with regolith materials could be detected in a shorter period of time using high energy prompt muons ($< 30 \text{ days}$; Fig. 13A).

Muons produced by the decay of pions and kaons could be used to image the interior of small bodies on the scale of a few 10s of meters in diameter. Muons with energies greater than a few 10s of GeV can penetrate asteroids of this size (Fig. 5C). The integral flux of muons produced by the decay of π , k mesons in this energy range is higher than that of prompt muons (Figs. 7 and 8). The detection limit for a 25-m diameter inclusion within a 50-m diameter asteroid as a function of inclusion density is shown in Fig. 13B. For a small asteroid, a large inclusion could be detected in a matter of hours. Assuming the transmitted muon flux can be separated from various sources of background, it is possible that interior regions could be radiographed.

HODOSCOPE DESIGN CONCEPTS

A practical hodoscope must separate the transmitted muons from the energetic particle background in the vicinity of the asteroid. For Earth applications, a hodoscope with two, position-sensitive planes can be used. It is safe to assume that most energetic charged particles at sea level

are muons and for the purpose of radiography any coincidence event can be counted as a muon (e.g. Tanaka et al., 2010a). In the vicinity of an asteroid, the particle population includes primary GCRs and scattered, secondary charged particles (e.g. electrons, protons, pions, etc...) that escape the surface in the direction of the hodoscope. A low energy population of secondary muons produced near the surface of the asteroid will also contaminate the measurements. Unless they can be rejected, the signatures from these other particles will obscure the faint signal from transmitted muons.

To illustrate the challenge faced in designing a hodoscope, we simulated the upward-going current of particles leaking away from the surface of a large asteroid (10 km diameter) (Fig. 14). With the exception of muons, the upward going particles are made in the outermost layer of the asteroid, within the top few meters. Consequently, the magnitude and energy distribution of these particles is not expected to vary much with asteroid diameter.

For comparison, the transmitted muon current for a 50-m diameter asteroid is shown (Fig. 14). The transmitted current was calculated for π , K muons with energies greater than 10 GeV. Below about 1-10 GeV, the magnitude of the transmitted current is smaller than the leakage current for all other particles. The transmitted muon current above 1 GeV is sensitive to density variations within the interior of the asteroid. An effective hodoscope design must be capable of cleanly separating this signal from the background.

There are many approaches that could be taken to separate the flux of muons greater than 1 GeV from the background. For example, a strong magnetic field could be used for this purpose; however, this would result in a large and expensive instrument. The Alpha Magnetic Spectrometer (AMS) uses superconducting magnets to produce a 0.15T field (Aguilar et al., 2005; Fig. 15). The hodoscope, which is immersed in the magnetic field, includes multiple tracking planes to determine the curvature of the charged particle trajectory. The gyroradius of a 1 GeV, singly-charged particle is about 20 m. Separation of energies based on the gyroradius would require very precise position information on the tracking planes, which would add to cost and complexity.

A Transition Radiation Detector (TRD), which can detect highly relativistic particles ($\gamma \geq 10^3$) (Nakamura et al., 2010) could be used to separate the high energy component of the transmitted

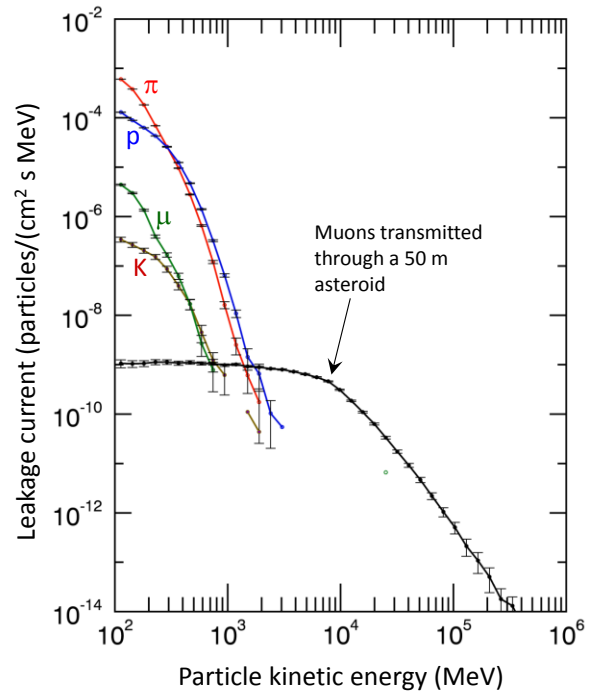


Figure 14. The upward going current of protons, pions, kaons, and muons from a large asteroid (10 km diameter) is shown. Only particles emitted within 45° of zenith contribute to the current. These would appear in the field of view of a hodoscope along with muons transmitted through the interior. Other than muons, the particles are emitted within the top few meters of the surface of the asteroid. The magnitude and energy distribution of the upward-going current is not expected to change with asteroid diameter. For comparison, the transmitted flux of muons, also within 45° of zenith, is shown for π , K muons produced in a 50-m diameter asteroid.

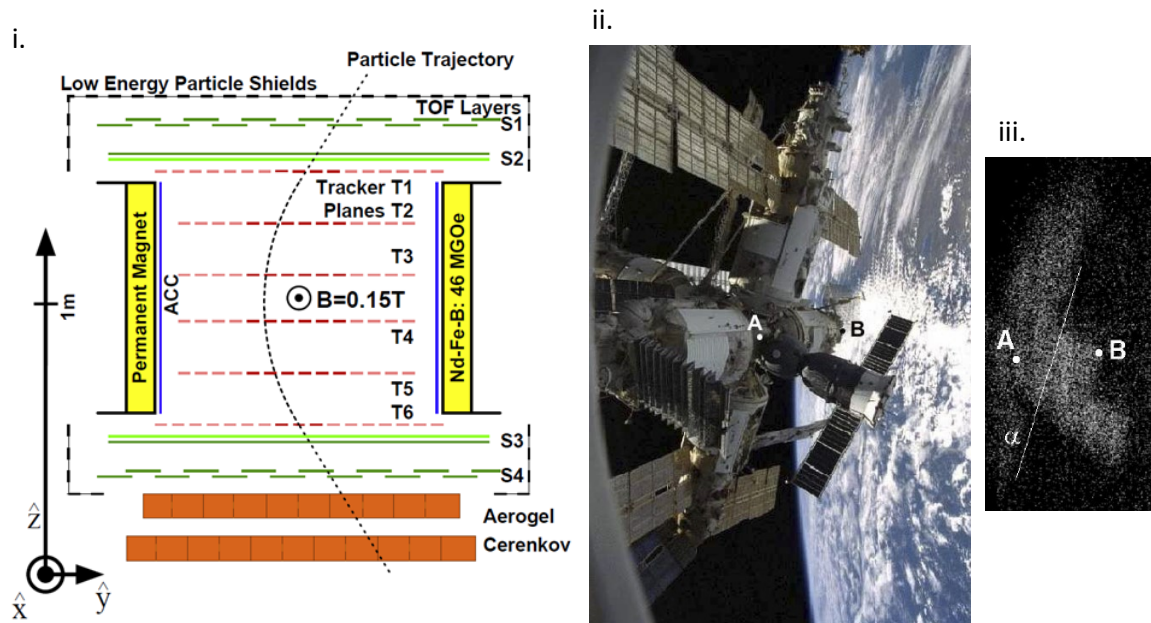


Figure 15. The Alpha Magnetic Spectrometer (AMS), deployed on the Space Shuttle, imaged low-energy, secondary pions and muons produced by GCR interactions with the Mir space station. A diagram of AMS (i) shows components that could be used in a practical telescope for muography of a small comet or asteroid. These include tracker planes (hodoscope) to determine particle direction and an array aerogel Cherenkov detectors for particle velocity selection. A photograph of the spacecraft (ii) is compared to an image of secondary pions and muons, which shows the outlines of the station and Soyuz capsule (iii) (the AMS diagram and images are from Aguilar et al., 2005).

muon flux from the background. TRDs detect x-rays produced when highly relativistic particles cross a refractive interface. X-rays less than several 10s of keV are made with a characteristic angle of $1/\gamma$ from the incident particle direction. To maximize x-ray production, multiple crossings are required, which can be accomplished using many thin foils of low-Z material or a micro-porous medium followed by position-sensitive x-ray sensor (ibid.). The TRD would act as a velocity selector and could filter out protons with kinetic energies below 1 TeV and pions, kaons, and muons with kinetic energies below about 100 GeV. The TRD would be used in conjunction with multiple tracking planes to determine particle direction and to reject coincident backgrounds. Some shielding would be required to filter out contributions from low energy particles. Downward-going particles could be rejected by time-of-flight. The main problem with TRDs is that the x-rays are produced with a small emission angle, virtually coincident with the charged particle trajectory such that ionization energy losses from the particle itself compete with the detection of the x-rays. Separating these components may result in added bulk and complexity. In addition, the threshold energy for particle detection is large such that no interior contrast would be observed for bodies less than about 100 m diameter (see the range-energy relationship in Fig. 5C). If a compact device can be made, this technique may be the most effective way to utilize high-energy muons produced by charmed mesons to image the interiors of larger asteroids.

Alternatively, a Cherenkov detector could be used as a velocity filter. A charged particle will radiate photons when it traverses a dielectric medium with speed in excess of the phase velocity of light in the medium. The Cherenkov photons can be detected, for example, using photomultiplier tubes or solid-state (silicon) photomultipliers. The criterion for the emission of Cherenkov radiation is $\beta n > 1$, where $\beta = v/c$ (ratio of the particle velocity to the speed of light in vacuum) and

n is the refractive index of the medium at the frequency of the emitted photons. For a proton with 1 GeV kinetic energy, $\beta = 0.875$. A dielectric with refractive index less than 1.14 would be needed to discriminate against protons < 1 GeV. For a muon with a kinetic energy of 1 GeV, $\beta = 0.9955$ and $n < 1.005$ would be required. Silica aerogels, which have the lowest refractive index of any known solid material, are used routinely as radiators for accelerators and space applications (e.g. Cantin et al., 1974, Higinbotham, 1998; Fig. 15), and can be selectively manufactured with an index of refraction between 1.006 and 1.06 (e.g. Iijima et al., 2005). The lower (1 GeV) threshold provided by Cherenkov detectors would enable imaging of the interior of a wider range of asteroid dimensions than could be accomplished with a TRD.

As with the TRD, a Cherenkov radiator could be used as a velocity filter in conjunction with multiple tracking planes to determine particle detection. Direction information can also be obtained from the angular distribution of the Cherenkov radiation, which can be measured precisely, for example, using a Ring Imaging Cherenkov detector (e.g. Akopov et al., 2002). The cosine of the emission angle of Cherenkov light is inversely proportional to particle velocity. Imaging of the Cherenkov photons would provide directional information, which could be used as a backup or in place of time-of-flight information used to discriminate between upward- or downward-going particles and to precisely determine their direction. Thus, a Cherenkov radiator could be used for both velocity selection and tracking.

The ability to survey the periphery of an asteroid as well as the deep interior may be desired. In this case, the acceptance of the hodoscope would need to be wider than that of a two-layer planar device. With scintillating fibers, a non-planar hodoscope with a wide field-of-view is possible.

Finally, we note that multiple muons are produced in a narrow cone during a cosmic ray showers. The detection of simultaneous parallel penetrating tracks may be a valid way to reject the background and uniquely identify muons from showers occurring on the opposite side of the object. This concept can be explored using the modeling tools available to our research team.

In future work, all of the potential detector techniques reviewed above can be considered in combinations that can provide the discrimination needed with sufficient efficiency as well as the highest reliability and lowest resource impact in terms of mass, power and telemetry bandwidth.

PILOT RADAR-MUOGRAPHY MISSION

Muon production occurs in the outer meter of an asteroid or comet surface and is sensitive to the bulk density of the material. Bulk density is a function of the density of solid (granular) material of this layer and its porosity. Radar affords a means by which near-surface bulk density can be determined for the outer meter (Magri et al. 2001). One method requires the assumption of solid density of grains corresponding to that of meteoritic material analogous to the target object by spectroscopic comparison. Porosity is then derived from the power in the returned circular polarizations (ibid.).

For tomographic purposes, both the detailed shape and the variation of bulk density over the surface must be determined. For some near-Earth object targets it is possible to do this remotely using ground-based radar installations, Arecibo and Goldstone, as has been demonstrated for the OSIRIS-Rex target 101955 Bennu (Nolan et al. 2013). Alternatively, a spacecraft-based radar system could also provide the same results at yet higher resolution.

Our pilot mission would identify and characterize the near surface density structure and shape of selected NEAs using radar observations. An easily accessible NEA would be selected and a spacecraft would deploy a hodoscope in close proximity to the asteroid. If a framing camera were included on the payload, radar shape data could be supplemented or confirmed via stereophotoclinometry. The spacecraft could also be equipped with a fast neutron detector to map regolith atomic mass to depths of a few decimeters while flying in formation with the asteroid. Atomic mass and density information would be used to correct muon radiographic data. As in the NEAR and OSIRIS-Rex missions, the spacecraft could touch down on the NEA surface acquire a muon radiograph over the period of a few months. Alternatively, tomographic data could be acquired in close proximity while flying in formation with the asteroid.

At a minimum, the mission would validate muon observations against measurements of bulk density and porosity derived from asteroid mass, volume and radar observations. We envision that the mission could be carried out within the scope of the NASA Discovery Program. The mission may also be within the reach of the commercial space industry, depending on the success of NEA mining endeavors now in progress.

CONCLUSIONS AND FUTURE WORK

We have completed all three tasks of our Phase I project: 1) *Source characterization*: Characterize the production of secondary particles made by cosmic ray showers in planetary surfaces and atmospheres; 2) *Imaging studies*: Determine the sensitivity of secondary particles to the composition and density structure of small solar-system bodies; 3) *Sensor design*: Identify the attributes of instruments that can detect and image secondary particles. A secondary goal to compare methods used for radiation transport calculations by three groups of researchers was also accomplished. This activity has led to improvements in modeling capabilities.

Muons, which are the long-range, charged-particle component of GCR showers, were identified as the most likely source of information about the deep interior of solid, airless bodies. We used Monte Carlo radiation transport codes MCNPX and FLUKA, benchmarked against experimental data acquired at sea level on Earth, to characterize the production of muons in the surfaces of asteroids and comets. Results of these calculations confirmed our scaling of Gaisser's semi-empirical model from Earth's atmosphere to solid, regolith materials. The models show that muon production, which occurs in the topmost meter of planetary regoliths, is over 3 orders of magnitude smaller than in Earth's atmosphere. In addition, we found that muon production by the decay of charged pions and kaons is a strong function of regolith density.

Despite the low intensity of muons, it may be possible to characterize the bulk porosity and internal structure of asteroids and comets. A search for high contrast interior regions (ice or iron-rich material beneath a silicate regolith) could be feasible for objects with 100- to 1-km diameters using prompt muons produced by the decay of charmed mesons (> 100 GeV). FLUKA calculations are consistent with other published studies (e.g. Bugaev et al., 1998) in predicting that prompt muons dominate the high-energy muon flux in solid surfaces. In addition, the production of prompt muons does not depend on regolith density. Consequently, the flux of transmitted, prompt muons is sensitive to interior structure rather than surface density variations once corrections for shape are made. Very small bodies (10- to 100-m in diameter) or surface features on a large, airless body (e.g. lava tubes within the lunar surface), could be imaged using muons produced by the decay of

charged pions and kaons, which are more abundant at low energies (between 10- and 100-GeV). The amount of time needed for interior mapping would range from a few weeks to a year, depending on the diameter of the object and depths of interest. The density of the regolith would need to be mapped (e.g. using radar) to properly account for variations in muon production.

The practical implementation of muography depends on the ability of the muon telescope (hodoscope) to separate the high-energy transmitted muons from various background sources. These include primary GCR particles (protons) and other energetic particles in the space environment as well as secondary particles originating within the surface on the same side of the asteroid as the hodoscope. The primary particles can be rejected using time-of-flight, to find out which way (up or down) the particle went through the hodoscope. The secondary background interferes with the transmitted muons at energies up to about 1 GeV. Screening of these particles using a velocity selector (e.g. Cherenkov counter or Transition Radiation Detector) may be an effective method for background rejection. A Cherenkov detector can also provide directional information for up-down discrimination or tracking. A practical hodoscope would likely consist of an anti-coincident shielding, a Cherenkov detector, and multiple tracking planes. While this notional design is more complex than Earth-based systems, which can be as simple as two position sensitive planes, we think that a compact (1 m²) hodoscope for asteroid muography could be constructed with relatively low mass, complexity and cost in comparison to the Alpha Magnetic Spectrometer.

Our Phase I study has identified many of the challenges that must be overcome in order to use muography to characterize the interior of small solar system bodies. Future studies will focus on a thorough assessment of the muon transmitted signal in comparison to backgrounds, with the goal of establishing specific design requirements for hodoscopes. In addition, the information content of the background sources will be examined. For example, Fig. 14 shows that the upward pion flux is comparable in magnitude to that of protons. If so, then measurements of the gross, charged-particle leakage flux may be sensitive to regolith density variations (the flux of charged pions varies with density), perhaps providing a simple means to characterize regolith density in situ along a rover traverse or from orbit. Aspects of hodoscope design need to be investigated in more detail, including modeling of instrument response to the transmitted muons and backgrounds and demonstrating that interior structure can be determined from the measurements. This activity would include the evaluation of different data acquisition scenarios and image reconstruction methods. Experimental evaluation of instrument components and subsystems can be carried out at accelerator facilities. If silica aerogel is to be used for the radiator, then some investigation of the practical limits of the index of refraction for this material is needed. A Phase II project would address most of these issues, further validating the feasibility and range of applicability of the proposed method, while advancing the instrument technology beyond TRL-2 (Mankins, 1995).

Finally, we have identified a pilot mission scenario to a near Earth asteroid, which could be implemented once the instrument technology has been demonstrated. The pilot mission would use Earth-based radar to map the regolith density and shape of a selected asteroid. A spacecraft could deploy a prototype hodoscope close to the surface of the asteroid to patiently acquire the first image of the interior structure. A Phase II project would include an initial study of the feasibility of this mission scenario.

While the practical implementation of muography must overcome many challenges, the potential benefits are considerable. At present, there is no established method to directly determine the

interior structure of small bodies; although, active seismology (e.g. Asphaug, 2008) and radar-based methods have been suggested. Such information is important for planetary science, in situ resource utilization, mining, and planetary defense. In closing, we note that the exploration of near-Earth objects is part of the Global Exploration Roadmap for human missions beyond low-Earth orbit (GER 2013). In support of this, NASA has generated a detailed list of Strategic Knowledge Gaps (SKGs) needed to be addressed to support human exploration. Macroscopic porosity of small body interiors is among these SKGs (NASA SBAG 2014). Interior structure is also critical to determine modes of planetary defense against a potentially hazardous object (e.g., Asphaug et al. 1998).

ACKNOWLEDGEMENTS

T. H. Prettyman acknowledges his affiliations with the University of New Mexico's Institute of Meteoritics and the NASA Jet Propulsion Laboratory, which provided some of the library resources needed to carry out this work. We are grateful to J. S. Hendricks for his assistance in modifying the MCNPX code.

REFERENCES

- Ahrens, T. J. and A. W. Harris (1992), Deflection and fragmentation of near-Earth asteroids, *Nature*, Vol. 360, pp. 429-433.
- Akopov, N. et al., HERMES RICH group (2002), The HERMES dual-radiator ring Imaging Cherenkov detector, *Nucl. Instrum. Meth. Phys. Res. A*, Vol. 479, Issues 2-3, pp. 511-530.
- Allkofer, O., K. Carstensen, W. D. Dau (1971), The absolute cosmic ray muon spectrum at sea level, *Physics Letters*, Vol. 36B, No. 4, pp. 425-427.
- Alvarez, L. W., J. A. Anderson, F. El Bedwei, J. Burkhard, A. Fakhry, A. Girgis, A. Goneid, F. Hassan, D. Iverson, G. Lynch, Z. Miligy, A. H. Moussa, M. Sharkawi, L. Yazolino (1970), Search for hidden chambers in the pyramids, *Science*, Vol. 167, pp. 832-839.
- Ambrosino, F., A. Anastasio, D. Basta, L. Bonechi, M. Brianzi, A. Bross, S. Callier, A. Caputo, R. Ciaranfi, L. Cimmino, R. D'Alessandro, L. D'Auria, C. de La Taille, S. Energico, F. Garufi, F. Giudicepietro, A. Lauria, G. Macedonio, M. Martini, V. Masone, C. Mattone, M.C. Montesi, P. Noli, M. Orazi, G. Passeggio, R. Peluso, A. Pla-Dalmau, L. Raux, P. Rubinov, G. Saracino, E. Scarlini, G. Scarpato, G. Sekhniadze, O. Starodubtsev, P. Strolin, A. Taketa, H.K.M. Tanaka, A. Vanzanella, L. Viliani (2014), The MU-RAY project: detector technology and first data from Mt. Vesuvius, *Journal of Instrumentation*, Vol. 9, C02029, doi:10.1088/1748-0221/9/02/C02029.
- Asphaug, E., S. J. Ostro, R. S. Hudson, D. J. Scheeres, W. Benz (1998), Disruption of kilometer-sized asteroids by energetic collisions, *Nature*, Vol. 393, pp. 437-440, doi: 10.1038/30911.
- Asphaug, E. (2008), Critical crater diameter and asteroid impact seismology, *Meteoritics & Planetary Science*, Vol. 43, Nr. 6, pp. 1075-1084
- Badhwar, G. D. and P. M. O'Neill (1996), Galactic cosmic radiation model and its applications, *Adv. Space Res.*, Vol. 17, No. 2, pp. (2)7-(2)17.

- Battistoni G., (2006), Recent developments in the FLUKA nuclear reaction models, Proceedings of 11th International Conference on Nuclear Reaction Mechanisms, Varenna.
- Battistoni G., Muraro S., Sala P. R., Cerutti F., Ferrari A., Roesler S., Fasso A., and Ranft J. (2007) The FLUKA code: Description and benchmarking. In Hadronic Shower Simulation Workshop (eds. M. Albrow and R. Raja), pp. 31-49. AIP Conference Proceeding.
- Battistoni G., Cerutti F., Empl A., Fassò A., Ferrari A., Gadioli E., Garzelli M., Muraro S., Pelliccioni M., Pinsky L. (2008) Hadronic models for cosmic ray physics: the FLUKA code, *Nuclear Physics B- Proceedings Supplements*, Vol. 175, pp. 88-95.
- Binzel, R. P. (2000), The Torino impact hazard scale, *Planetary and Space Science*, Vol. 48, Issue 4, pp. 297-303.
- Borozdin K. N., Hogan G. E., Morris C., Priedhorsky W. C., Saunders A., Schultz L. J., and Teasdale M. E. (2003) Surveillance: Radiographic imaging with cosmic-ray muons. *Nature*, Vol. 422, No. 6929, 277-277.
- Borozdin, K., S. Greene, Z. Lukić, E. Milner, H. Miyadera, C. Morris, J. Perry (2012), Cosmic ray radiography of the damaged cores of the Fukushima reactors, *Phys. Rev. Lett.*, Vol. 109, 152501, doi: 10.1103/PhysRevLett.109.152501.
- Boynton W., Feldman W., Squyres S., Prettyman T., Brückner J., Evans L., Reedy R., Starr R., Arnold J., and Drake D. (2002) Distribution of hydrogen in the near surface of Mars: Evidence for subsurface ice deposits. *Science*, Vol. 297(5578), pp. 81-85.
- Brown, P. G., J. D. Assink, L. Astiz, R. Blaauw, M. B. Boslough, J. Borovička, N. Brachet, D. Brown, M. Campbell-Brown, L. Ceranna, W. Cooke, C. de Groot-Hedlin, D. P. Drob, W. Edwards, L. G. Evers, M. Garces, J. Gill, M. Hedlin, A. Kingery, G. Laske, A. Le Pichon, P. Mialle, D. E. Moser, A. Saffer, E. Silber, P. Smets, R. E. Spalding, P. Spurný, E. Tagliaferri, D. Uren, R. J. Weryk, R. Whitaker, Z. Krzeminski (2013), A 500-kiloton airburst over Chelyabinsk and an enhanced hazard from small impactors, *Nature*, Vol. 503, pp. 238-241, doi: 10.1038/nature12741.
- Bugaev, E. V., A. Misaki, V. A. Naumov, T. S. Sinegovskaya, S. I. Sinegovsky, N. Takahashi (1998), Atmospheric muon flux at sea level, underground, and underwater, *Phys. Rev. D*, Vol. 58, 054001, DOI: 10.1103/PhysRevD.58.054001.
- Cantin, M., M. Casse, L. Koch, R. Jouan, P. Mestreau, D. Roussel (1974), Silica aerogels used as Cherenkov detectors, *Nucl. Instrum. Meth.*, Vol. 118, Issue 1, pp. 177-182.
- Coan, T., T. Liu, J. Ye (2006), A compact apparatus for muon lifetime measurement and time dilation demonstration in the undergraduate laboratory, *Am. J. Phys.*, Vol. 74, 161, doi: 10.1119/1.2135319.
- Evans L. G., Starr R. D., Brückner J., Reedy R. C., Boynton W. V., Trombka J. I., Goldsten J. O., Masarik J., Nittler L. R., and McCoy T. J. (2001) Elemental composition from gamma-ray spectroscopy of the NEAR-Shoemaker landing site on 433 Eros. *Meteoritics & Planetary Science*, Vol. 36(12), 1639-1660.
- Fassò, A., A. Ferrari and J. Ranft and P. R. Sala (2001), FLUKA: Status and Perspectives for Hadronic Applications. Proceedings of the Monte Carlo 2000 Conference, Lisbon, pp. 159-164.

- Fass`, A., A. Ferrari and J. Ranft and P. R. Sala (1995), FLUKA, Performances and applications in the intermediate energy range. Proceedings of the Specialists' Meeting on Shielding Aspects of Accelerators, Targets & Irradiation Facilities, Arlington.
- Feldman W. C., Maurice S., Binder A. B., Barraclough B. L., Elphic R. C., and Lawrence D. J. (1998) Fluxes of Fast and Epithermal Neutrons from Lunar Prospector: Evidence for Water Ice at the Lunar Poles, *Science* Vol. 281(5382), pp. 1496-1500.
- Feldman W., Lawrence D., Elphic R., Vaniman D., Thomsen D., Barraclough B., Maurice S., and Binder A. (2000) Chemical information content of lunar thermal and epithermal neutrons. *Journal of Geophysical Research*, Vol. 105(E8), pp. 20347-20363.
- Ferrari A., P. R. Sala (1998), Intermediate and high energy models in FLUKA: Improvements, benchmarks and applications . Proceedings of Workshop on Nuclear Reaction Data and Nuclear Reactors Physics, Design and Safety, Trieste.
- Ferrari A., Sala P. R., Fasso A., and Ranft J. (2005), FLUKA: A multi-particle transport code, European Organization for Nuclear Research document CERN-2005-010.
- Fujiwara, A., J. Kawaguchi, D. K. Yeomans, M. Abe, T. Mukai, T. Okada, J. Saito, H. Yano, M. Yoshikawa, D. J. Scheeres, O. Barnouin-Jha, A. F. Cheng, H. Demura, R. W. Gaskell, N. Hirata, H. Ikeda, T. Kominato, H. Miyamoto, A. M. Nakamura, R. Nakamura, S. Sasaki, K. Uesugi (2006), The rubble-pile asteroid Itokawa as observed by Hayabusa, *Science*, Vol. 312, pp. 1330-1334.
- Gaisser, T. K., Cosmic Rays and Particle Physics, Cambridge University Press 1990, ISBN 0-521-32667-2.
- Goldader, J. D. and S. Choi (2010), An inexpensive cosmic ray detector for the classroom, *Phys. Teach.*, Vol. 48, 594, doi: 10.1119/1.3517025.
- Harrington T. M., Marshall J. H., Arnold J. R., Peterson L. E., Trombka J. I., and Metzger A. E. (1974) The Apollo gamma-ray spectrometer, *Nuclear Instruments and Methods*, Vol. 118(2), pp. 401-411.
- Hartmann, W. K., The resource base in our solar system, in Interstellar Migration and the Human Experience, B. R. Finney and E. M. Jones, Eds., University of California Press, Berkely and Los Angeles, California, 1985.
- Higinbotham, D. W. (1998), Diffusively reflective aerogel Cherenkov detector simulation techniques, *Nucl. Instrum. Meth. Phys. Res. A*, Vol. 414, pp. 332-339.
- Hudson, R. S. and S. J. Ostro (1995), Shape and non-principal axis spin state of asteroid 4179 Toutatis, *Science*, Vol. 270, No. 5233, pp. 84-86.
- Iijima, T. et al. (2005), A novel type of proximity focusing RICH counter with multiple refractive index aerogel radiator, *Nucl. Instrum. Meth. Phys. Res. A*, Vol. 548, Issue 3, pp. 383-390.
- Kalmykov N., Konstantinov A., Mukhamedshin R., Podorozhnyi D., Sveshnikova L., Turundaevskiy A., Tkachev L., and Chubenko A. (2011), Study of high energy cosmic rays by different components of back scattered radiation generated in the lunar regolith. In 32nd International Cosmic Ray Conference, Beijing.

- Kargel, J. S. (1994), Metalliferous asteroids as potential sources of precious metals, *J. Geophys. Res.*, Vol. 99, E10, 21129-21141, doi: 10.1029/94JE02141.
- Kedar, S., H. K. M. Tanaka, C. J. Naudet, C. E. Jones, J. P. Plaut, F. H. Webb (2013), Muon radiography for exploration of Mars geology, *Geosci. Instrum. Method. Data Syst.*, Vol. 2, pp. 157–164, doi:10.5194/gi-2-157-2013.
- Lesparre N., Gibert D., Marteau J., Déclais Y., Carbone D., and Galichet E. (2010) Geophysical muon imaging: feasibility and limits, *Geophysical Journal International*, Vol. 183, No. 3, pp. 1348-1361, doi: 10.1111/j.1365-246X.2010.04790.x.
- Lawrence D. J., Feldman W. C., Goldsten J. O., Maurice S., Peplowski P. N., Anderson B. J., Bazell D., McNutt R. L., Nittler L. R., Prettyman T. H., Rodgers D. J., Solomon S. C., and Weider S. Z. (2013) Evidence for Water Ice Near Mercury's North Pole from MESSENGER Neutron Spectrometer Measurements, *Science* Vol. 339(6117), pp. 292-296.
- Lingenfelter R. E., Canfield E. H., and Hess W. N. (1961), The lunar neutron flux, *Journal of Geophysical Research*, Vol. 66(9), pp. 2665-2671.
- Lipari, P. (1993), Lepton spectra in the earth's atmosphere, *Astroparticle Physics*, Vol. 1, pp. 195-227.
- Longman, A., Growth Adapted Tensegrity Structures - A New Calculus for the Space Economy, NASA Innovative Advance Concepts project website, <http://www.nasa.gov/content/growth-adapted-tensegrity-structures-a-new-calculus-for-the-space-economy>, 2013.
- Magri, C., G. J. Consolmagno, S. J. Ostro, L. A. M. Benner, B. R. Beeny (2001), Radar constraints on asteroid regolith properties using 433 Eros as ground truth, *Meteorit. Planet. Sci.*, Vol. 36, pp. 1697-1709.
- Mankins J. C. (1995) Technology readiness levels. White Paper, April 6.
- Mashnik S., Gudima K., Moskalenko I., Prael R., and Sierk A. (2004), CEM2K and LAQGSM codes as event generators for space-radiation-shielding and cosmic-ray-propagation applications, *Advances in Space Research*, Vol. 34, No. 6, pp. 1288-1296.
- Marteau, J. D. Gilbert, N. Lesparre, F. Nicollin, P. Noli, F. Giacoppo (2012), Muons tomography applied to geosciences and volcanology, *Nucl. Instrum. Meth. Phys. Res. A*, Vol. 695, pp. 23-28, <http://dx.doi.org/10.1016/j.nima.2011.11.061>.
- McKinney G., Lawrence D., Prettyman T., Elphic R., Feldman W., and Hagerty J. (2006), MCNPX benchmark for cosmic ray interactions with the Moon, *J. Geophys. Res.*, Vol. 111, E6, E06004.
- Menichelli, M., S. Ansoldi, M. Bari, M. Basset, R. Battiston, S. Blasko, F. Coren, E. Fiori, G. Giannini, D. Iugovaz A. Papi, S. Reia, G. Scian (2007), A scintillating fibres tracker detector for archaeological applications, *Nucl. Instrum. Meth. Phys. Res. A*, Vol. 572, Issue 1, pp. 262–265.
- Miller, R. S. and D. J. Lawrence, Muon radiography as a probe of the interior structure of small solar system bodies, 45th Lunar and Planetary Science Conference, 17-21 March, 2014, Abstract #1134.

- Miyadera, H., K. N. Borozdin, S. J. Greene, Z. Lukić, K. Masuda, E. C. Milner, C. L. Morris, J. O. Perry (2013), Imaging Fukushima Daiichi reactors with muons, *AIP Advances*, Vol. 3, 052133, doi: 10.1063/1.4808210.
- NASA NEO Program, NASA Near Earth Object Program website, <http://neo.jpl.nasa.gov/risk/>.
- NASA SBAG, NASA Small Bodies Assessment Group 2014. Strategic Knowledge Gaps database. <http://www.lpi.usra.edu/sbag/documents/>.
- Nakamura, K. et al. (Particle Data Group) (2010), Review of Particle Physics, *J. Phys. G: Nucl. Part. Phys.*, Vol. 37, 0075021, doi:10.1088/0954-3899/37/7A/075021.
- Nolan, M.C., C. Magri, E.S. Howell, L.A.M. Benner, J.D. Giorgini, C.W. Hergenrother, R.S. Hudson, D.S. Laretta, J.-L. Margot, S.J. Ostro and D.J. Scheeres 2013. Shape model and surface properties of the OSIRIS-REx target Asteroid (101955) Bennu from radar and lightcurve observations. *Icarus* 226, 629-640.
- Okubo, S. and H. K. M. Tanaka (2012), Imaging the density profile of a volcano interior with cosmic-ray muon radiography combined with classical gravimetry, *Meas. Sci. Technol.*, Vol. 23, pp. 1-16, doi:10.1088/0957-0233/23/4/042001.
- O’Niell, G. K., *The High Frontier: Human Colonies in Space*, William Morrow & Company, New York, 1977, ISBN 0-688-03133-1.
- Pelowitz D. B., Durkee J. W., Elson J. S., Fensin M. L., Hendricks J. S., James M. R., Johns R. C., McKinney G. W., Mashnik S. G., Verbeke J. M., Waters L. S., and Wilcox T. A. (2011), MCNPX 2.7.0 Extensions. Los Alamos National Laboratory document LA-UR-11-02295.
- Pfotzer (1936), Dreifachkoinzidenzen der Ultrastrahlung aus vertikaler Richtung in der Stratosphäre, *Z. Physik*, Vol. 102, Issue 1-2, pp. 41-58.
- Prettyman T. H., Feldman W. C., Mellon M. T., McKinney G. W., Boynton W. V., Karunatillake S., Lawrence D. J., Maurice S., Metzger A. E., Murphy J. R., Squyres S. W., Starr R. D., and Tokar R. L. (2004) Composition and structure of the Martian surface at high southern latitudes from neutron spectroscopy. *J. Geophys. Res.* Vol. 109(E5), E05001.
- Prettyman T. H., Feldman W., McSween H., Dingler R., Enemark D., Patrick D., Storms S., Hendricks J., Morgenthaler J., Pitman K., and Reedy R. (2011) Dawn’s Gamma Ray and Neutron Detector. *Space Science Reviews* 163(1), 371-459.
- Prettyman T. H., Mittlefehldt D. W., Yamashita N., Lawrence D. J., Beck A. W., Feldman W. C., McCoy T. J., McSween H. Y., Toplis M. J., Titus T. N., Tricarico P., Reedy R. C., Hendricks J. S., Forni O., Le Corre L., Li J.-Y., Mizzon H., Reddy V., Raymond C. A., and Russell C. T. (2012) Elemental Mapping by Dawn Reveals Exogenic H in Vesta’s Regolith. *Science* Vol. 338(6104), pp. 242-246.
- Prettyman, T. H., S. L. Koontz, L. S. Pinsky, A. Empl, W. Mendell, D. W. Mittlefehldt, B. D. Reddell, M. V. Sykes, Deep mapping of small solar system bodies with galactic cosmic ray secondary particle showers, *NASA Innovative Advanced Concepts Symposium*, Stanford University, Feb. 5, 2014, <http://www.nasa.gov/content/deep-mapping-of-small-solar-system-bodies-with-galactic-cosmic-ray-secondary-particle/>.
- Tanaka, H. K. M., T. Nakano, S. Takahashi, J. Yoshida, M. Takeo, J. Oikawa, T. Ohminato, Y. Aoki, E. Koyama, H. Tsuji, K. Niwa (2007), High resolution imaging in the inhomogenous crust with

cosmic-ray muon radiography: The density structure below the volcanic crater floor of Mt. Asama, Japan, *Earth and Planetary Science Letters*, Vol. 263, pp. 104-113.

Tanaka, H. K. M., T. Nakano, S. Takahashi, J. Yoshida, M. Takeo, J. Oikawa, T. Ohminato, Y. Aoki, E. Koyama, H. Tsuji, H. Ohshima, T. Maekawa, H. Watanabe (2008), Radiographic imaging below a volcanic crater floor with cosmic-ray muons, *American Journal of Science*, Vol. 308, pp. 843-850, doi:10.2475/07.2008.02.

Tanaka, H. K. M., T. Uchida, M. Tanaka, H. Shinohara, H. Taira (2009), Cosmic-ray muon imaging of magma in a conduit: Degassing process of Satsuma-Iwojima volcano, Japan, *Geophysical Research Letters*, Vol. 36, L01304, doi:10.1029/2008GL036451.

Tanaka, H. K. M., T. Uchida, M. Tanaka, H. Shinohara, H. Taira (2010a), Development of a portable assembly-type cosmic-ray muon module for measuring the density structure of a column of magma, *Earth Planets Space*, Vol. 62, pp. 119-129.

Tanaka, H. K. M., H. Taira, T. Uchida, M. Tanaka, M. Takeo, T. Ohminato, Y. Aoki, R. Nishitama, D. Shoji, H. Tsuiji (2010b), Three-dimensional computational axial tomography scan of a volcano with cosmic ray muon radiography, *J. Geophys. Res.*, Vol. 115, B12332, doi:10.1029/2010JB007677.

Tanaka, H. K. M. (2012), Evaluation of positioning and density profiling accuracy of muon radiography by utilizing a 15-ton steel block, *Geosci. Instrum. Method. Data Syst. Discuss.*, Vol. 2, pp. 643-656, doi:10.5194/gid-2-643-2012.

GER, The Global Exploration Roadmap 2013. International Space Exploration Coordination Group.

Veverka, J. et al. (2001), Imaging of small-scale features on 433 Eros from NEAR: Evidence for a complex regolith, *Science*, Vol. 292, pp. 484-488.

Weissman, P. R., E. Asphaug, S. C. Lowry, Structure and density of cometary nuclei, *Comets II*, M. Festou, H. U. Keller, H. A. Weaver, Eds., University of Arizona Press, 2004.

Yamashita N., Gasnault O., Forni O., d'Uston C., Reedy R., Karouji Y., Kobayashi S., Hareyama M., Nagaoka H., and Hasebe N. (2012) The global distribution of calcium on the Moon: Implications for high-Ca pyroxene in the eastern mare region, *Earth and Planetary Science Letters* Vol. 353, pp. 93-98.